"Clays for Our Future", H. Kodama, A.R. Mermut, and J.K. Torrance (eds.)
Proceedings of the 11th International Clay Conference, Ottawa, Canada, 1997.
Published by the ICC-97 Organizing Committee, Ottawa, Canada (1999) pp. 825.
ISBN 0-9686314-0-7.

Mineralogical analysis of a loess/paleosol couplet from the Chinese loess plateau

M.-Z. Dang[1], D.G. Rancourt[1], G. Lamarche[1] and M.E. Evans[2]

[1]Department of Physics, University of Ottawa, Ottawa, Ontario, Canada K1N 6N5;
[2]Institute of Geophysics, Meteorology and Space Physics, University of Alberta, Edmonton, Alberta, Canada T6G 2J1

We have used several complementary techniques to perform mineralogical, chemical, and magnetic characterizations of samples from the S3/L4 couplet of the loess/paleosol section at Baoji, China. Our approach combines: powder X-ray diffraction, X-ray fluorescence analysis, light element analyses, magnetometry, and Fe-57 Mössbauer spectroscopy. We find that the main pedogenic (i.e., abundant in S3 but not in L4) oxide that is magnetically ordered at room temperature is not stoichiometric magnetite but that a probable mixture of non-stoichiometric hydrous hematite, maghemite, and some non-stoichiometric (oxidized) magnetite is much more abundant. We also find: a high degree of vertical homogeneity in the original parent material across S3/L4, a more advanced stage of pedogenic development in the paleosol in which the Fe is distributed from the layer silicate minerals to the pedogenic oxides, and pedogenic and paleo-weathering influences on the distributions of Ca, P, C, Na and K.

Key words: China, Baoji, loess, paleosol, magnetism, maghemite, magnetite, hematite, Mössbauer spectroscopy, mineralogical characterization

INTRODUCTION

It is now well established that the loess deposits of central China provide a continuous record of global climate changes over the last 2.5 Ma and that it is the most complete such land-based record (Beer *et al.* 1993; Bronger and Heinkele 1990; Heller and Evans 1995; Kukla 1987; Kukla and An 1989; Rutter *et al.* 1991; and references therein). Climatic oscillations are marked by alternating loess and paleosol units that originated from similar wind-blown silt deposits which evolved, to different degrees, into soils, depending on the prevailing paleoclimatic conditions. Since the climatic changes were abrupt, the boundaries between loess units (dry grassland soils) and paleosol units (humid warm forest soils) are well defined and allow continuous stratigraphy to be based on simple field observations of associated properties such as colour, presence of fossils, and magnetic susceptibility. The field observations are further supported by laboratory tests involving: pollen counts, granulometry, magnetometry, oriented remanent magnetization measurements, isotope ratio determinations, chemical analyses, detailed morphological observations, Mössbauer spectroscopy, thermoluminescence dating, etc.

Dating has been established by the observed geomagnetic polarity changes (Heller and Evans 1995) and by strong correlations between the magnetic susceptibility data and the oxygen isotope record of deep-sea sediments (Kukla 1987). Interpretation is complicated by some loss of loess/paleosol boundary resolution due to bioturbation (roots, worms, snails, small burrowing mammals) and weathering (e.g., leaching of carbonate by percolating rainwater). In addition, there is significant variability from one loess (or paleosol) unit to the next, due to the dependencies of pedogenic activity, weathering, and deposition rates on climatic conditions.

On the one hand, the latter complexities offer an enormous amount of information about specific paleoclimatic periods but, on the other hand, they have impeded efforts to see the big picture, in terms of arriving at reliable stratigraphic dating. In this respect, magnetic measurements have been particularly useful. In addition to key magnetostratigraphy work from remanent magnetization, susceptibility data has allowed direct correlation with deep-sea sediment results, more refined boundary definitions, and sub-unit resolution of relatively minor climatic changes.

Magnetic susceptibility has emerged as a high-resolution climate proxy. Some recent efforts have been aimed at determining the mechanism or mechanisms that determine the susceptibility. Several models have been proposed that include: (a) compaction by differential weathering or leaching, (b) dilution by varying differential deposition rates for far and near sources, (c) pedogenic formation of magnetic iron oxides, and (d) formation of magnetic oxides by natural fires [see Heller and Evans (1995) and Eyre and Shaw (1994) for discussions]. Model-a has been ruled out in that it cannot alone explain the large magnitude of magnetic enhancement in the paleosols. Model-b has been ruled out in that the main mineral magnetic carriers (ferrimagnetic oxides) have been found to be very different in the loess and paleosol units. Indeed, whereas a greater fraction of the carriers in the loess (magnetite) is lithogenic, a larger fraction of the carriers in the paleosols has mineral and magnetic characteristics of

pedogenic iron oxide species, that may have been modified by natural fires. Although magnetite (both lithogenic and non-lithogenic) is certainly present and although some evidence suggests that magnetite is the main carrier of the magnetic susceptibility, it is possible that other mineral species such as pedogenic maghemite and hematite contribute more significantly.

It should be possible, by detailed mineralogical characterizations, to determine the precise physical cause(s) of magnetic enhancement in the paleosols. This would, in turn, lead to the mechanism(s) whereby the magnetic carriers were formed or accumulated, which, in turn, allow one to establish the particular climatic property(ies) that are recorded in the susceptibility signal. For example, does the susceptibility primarily measure: dominant wind patterns, or average rainfall, or average temperature, or frequency and intensity of natural fires, etc.? In addition, the detailed mineralogical data itself must contain much more information about each climatic period than that which can be deduced from single indicators such as magnetic susceptibility. Such indicators are convenient and economic simplifiers that allow vast temporal and spatial analyses but they cannot substitute for detailed mineralogical and morphological studies.

In the present paper we present preliminary results of detailed mineralogical, chemical, and magnetic analyses of two samples from the S3/L4 couplet of the Chinese loess plateau. We use several complementary techniques and report a comparative quantitative mineralogical phase analysis. This was achieved by combined powder X-ray diffraction (XRD), X-ray fluorescence (XRF) spectroscopy elemental analysis, and light element analysis for C, H, and N. In addition, we specifically studied the iron-bearing and magnetic phases by Mössbauer spectroscopy, magnetic separation, and cryogenic SQUID magnetometry.

SAMPLES AND EXPERIMENTAL METHODS

Our samples are from the Baoji section, were the S3-paleosol unit is 3.0 m thick, on top of the L4-loess unit which is 5.3 m thick. Our S3 sample was collected 1.0 m below the top of the S3 unit, in the subunit denoted Bt1 by Rutter *et al.* (1991) or LL1 by Kukla and An (1989). Our L4 unit was collected 5.6 m below the top of the S3 unit, in the subunit denoted C1 by Rutter *et al.* (1991). Kukla and An have not divided L4 into subunits. We chose the S3/L4 couplet at Baoji to start because this couplet has already been the object of both a high resolution susceptibility study (Evans *et al.* 1996) and a detailed granulometric study (Ding *et al.* 1994). In addition, it shows a high contrast between the loess and its associated paleosol and other studies have also concentrated on this couplet (Evans and Heller 1994; Hus and Bater 1993).

Room temperature (RT = 22° C) Fe-57 Mössbauer spectra were collected in transmission mode using random orientation powder absorbers having 95 mg of sample per cm^2 in holders with 1/2 inch diameter windows. Calibration was obtained using an enriched Fe-57 foil at RT and all RT center shifts (CSs) and line positions are reported with respect to the CS of metallic iron at RT. The transducer was operated in constant acceleration mode and folding was performed to achieve a flat background. All Mössbauer spectra were fit with the Rancourt-Ping Voigt-based fitting method for hyperfine field distributions (HFDs) (Rancourt and Ping 1991).

The X-ray diffractograms were collected using an automated Philips X'Pert PW3710 system powder diffractometer with rotating acetone smear on a single-crystal silicon wafer low-background holder. CuKα radiation was used.

The SQUID magnetometry measurements were performed on a low-field dc SQUID magnetometer that has been described elsewhere (Lamarche 1989). Typically ~ 10 mg of powder sample was immobilized in the cryogenic holder. The sample was first zero-field quenched (Earth's field), then the field was turned on (typically 10-100 Gauss) and the magnetic moment on the sample was measured on warming (field warming, FW). After the maximum temperature was reached, one could choose to measure as the sample was recooled (field cooling, FC).

Major and selected trace elements were analyzed on a Philips PW 2400 sequential XRF spectrometer, using fused glass disk sample preparation. The light element analyses for C, H, and N were performed by gas chromatography of the combustion products, on a Perkin Elmer PECHN 4000 elemental analysis system.

RESULTS AND DISCUSSION

The XRD diffractograms for the bulk L4 and S3 samples are shown in Fig. 1. Several strong reflections are unambiguously attributed to the majority phases: quartz (Qtz), plagioclase (Pl), microcline (Mc), chlorite (Chl), and illite (I11). In addition, the strongest reflection 104 of hematite (Hem) is resolved in both S3 and L4 (at $2\theta = 33.2$ degrees, $d = 2.70$ Å) and the 104 calcite (Cal) line is clearly seen in S3 ($2\theta = 29.5$ degrees, $d = 3.03$ Å).

The results from the XRF analyses are given in Table 1. By combining the XRD and XRF results, it is possible to calculate the majority phase abundances. The bulk mineralogy of S3 and L4 is fairly similar and can be described as: ~ 36 wt% quartz, ~ 20 wt% feldspars (both plagioclase and microcline together), ~ 18-24 wt% chlorite, and ~ 14-20 wt% illite [including muscovite (Ms) and all other mica-like phases]. The percentages by weight of the resistant index minerals (quartz and feldspar) for S3 and L4 are equal within error. This demonstrates a remarkable vertical homogeneity of the original parent material across this couplet. We are in the process of performing more accurate quantitative calculations, however, our preliminary

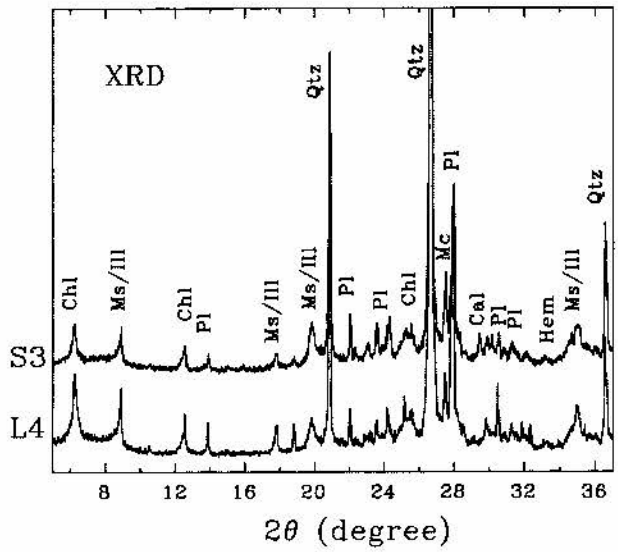

Fig. 1. XRD diffractograms for whole samples S3 and L4. Key reflections are identified with standard mineral symbols. Both diffractograms were collected under identical experimental conditions in the 2θ range 2-100 degrees but only an expanded section is shown.

results (Fig. 1) suggest that L4 contains more chlorite and illite than S3. This is consistent with S3 containing more (poorly crystalline) iron oxides, since total Fe is the same for both units (Table 1).

High resolution XRD scans were also run, in the 2θ range 33-38 degrees where the most intense reflection 100 of magnetite is expected to be resolved. These showed evidence for the magnetite reflection in the form of a weak shoulder on a neighbouring illite peak, occurring in both L4 and S3 and being larger in S3 but comparable. This, and the SQUID magnetometry data presented below, give conclusive proof of the presence of magnetite however it is not the most abundant oxide in either L4 or S3 (see below).

The bulk XRF results (Table 1) not only allow a semi-quantitative phase analysis but also show key differences in elemental compositions between S3 and L4. First, S3 has more Ca than L4 (~ 50 % more). This is the reverse from what is normally observed. That is, in general, loess units have higher Ca contents than associated paleosol units. The usual trend is explained in terms of dissolution, transport, and re-precipitation via the action of rain water, given that Ca is expected to be more labile in a soil. Our reverse situation may be due to the fact that our S3 sample is from LL1, a loess subunit of S3, if the overlying paleosol subunit of S3 had originally been particularly Ca rich and most Ca re-precipitation occurred in LL1. The XRF analyses were repeated to ensure that samples had not been exchanged by error in the first run.

Second, L4 has more P than S3 (about 70 % more). To our knowledge, this is the first report of a systematic difference in P between loess and paleosol units. Phosphorus is an essential nutrient for microorganisms and plants so we expect a larger fraction of available P to be metabolized in a soil having a larger biomass. Therefore, more of the original mineral P is expected to become labile via metabolization in a rich soil. It can then be lost to the underlying loess by rain water seepage. This is the same mechanism that makes loess units relatively Ca rich, although

Table 1. XRF results [wt % (oxides) or ppm (elements)]

Oxide/element	L4	L4rep	S3	S3rep
	wt %	wt %	wt %	wt %
SiO_2	64.33	63.36	63.58	63.08
TiO_2	0.77	0.770	0.787	0.783
Al_2O_3	14.92	14.99	15.06	15.02
Fe_2O_3	6.03	6.05	6.07	6.10
MnO	0.114	0.107	0.112	0.106
MgO	2.12	2.11	1.95	1.94
CaO	1.07	1.07	1.46	1.65
Na_2O	1.37	1.338	1.21	1.168
K_2O	2.792	2.795	2.705	2.688
P_2O_5	0.176	0.175	0.112	0.109
	ppm	ppm	ppm	ppm
V	100	98	102	104
Co	14	16	13	17
Cr	83	81	86	86
Ni	49	45	43	42
Zn	93	98	76	79
Rb	130	128.8	135	133.4
Sr	174	177.1	164	166.6
Y	37	36.9	38	38.3
Zr	227	227.3	239	237.2
Nb	18	17.1	20	19.2
Ba	576	556	549	578
La	<60	41	<60	37
Ce	90	101	72	84
Nd	<60	42	<60	36
Pb	44	49	30	44
Th	13	13.8	15	14.1
U	<10	7.0	<10	9.5
Ga	19	18	19	19
TOTAL	93.91	93.987	93.26	92.863
LOI	6.22	6.59	7.1	7.46
TOTAL	100.13	100.577	100.36	100.323

(*) Weight contributions of trace elements are included in total by use of corresponding assumed oxides.
LOI = loss on ignition. ppm are per mass units.

the dissolution and re-precipitation kinetics are expected to be different. Also, for both Ca and P, the established fact that the soils developed during periods of more abundant rainfall may be as important or more important than the relative action of metabolization. In other words, the extra rainfall would have simply washed away most Ca and P minerals.

Finally, the XRF results (Table 1) show that the loss on ignition (L-O-I) is about 1 wt% larger in S3 than in L4. This is consistent with the paleosol containing more residual organic compounds. This is substantiated by our light element analyses that gave total C contents of 0.14(4) and 0.44(4) wt% for L4 and S3, respectively. In particular, this amount of carbon in S3 is too large (by about 40%) in relation to the total Ca of S3, assuming all Ca is in calcite ($CaCO_3$) as suggested by the strong calcite reflection seen by XRD for S3 (Fig. 1). On the other hand, the difference in total Ca (Table 1) is not so great, such that an observable calcite signal should be present in the XRD pattern of L4, if all Ca were indeed in calcite. This suggests that the fraction of Ca not in calcite is larger in L4 than in S3. The other light element determinations gave H contents near the detection limit of 0.4 wt% and total N equal to zero within the accuracy of 0.4 wt%, for both S3 and L4.

The RT Mössbauer spectra of the bulk S3 and L4 samples are shown in Fig. 2. These are similar to spectra reported in previous studies (Eyre and Dickson 1995; Vandenberghe *et al.* 1992; Vandenberghe *et al.* 1998; and references therein). In this preliminary study, we have preferred to concentrate on bulk samples rather than the magnetic fractions, in order to avoid magnetic enrichment uncertainties in our quantitative phase analyses. We have also chosen to work on an associated couplet from the same site, in order to avoid problems related to both lateral deposition inhomogeneities and lateral paleoclimatic differences.

The spectra (Fig. 2) clearly show that, at RT, most of the Fe is in paramagnetic mineral species in both S3 and L4, although the ratio of Fe in magnetically ordered mineral species to total Fe in all mineral species (i.e., the hyperfine split to total spectral area ratio) is significantly different, being 11 % in L4 and 23 % in S3. This is in agreement with the well known enhanced magnetism of the paleosol.

The paramagnetic Fe-bearing mineral species mostly contain ferric iron. The RT paramagnetic ferrous iron content is approximately 13 % of total Fe for both L4 and S3. The CSs and quadrupole splittings of the paramagnetic doublets are consistent with: Fe-bearing chlorite, Fe-bearing micas including illite, and superparamagnetic (SP) or paramagnetic iron oxides and oxyhydroxides such as SP hematite, SP maghemite, ferrihydrite, akaganeite, and lepidocrocite.

The spectral contributions from magnetically ordered Fe-bearing species have large hyperfine magnetic field splittings that are typical of most bulk iron oxides and

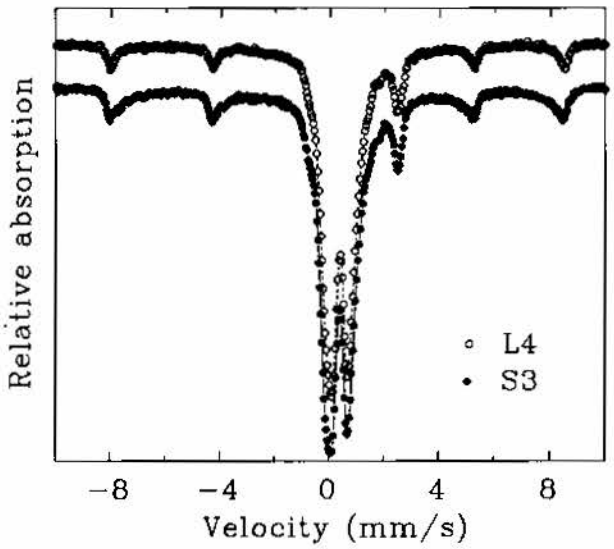

Fig. 2. RT Fe-57 Mössbauer spectra for whole samples S3 and L4.

oxyhydroxides. This is shown in Figs. 3(a) and (b) where the outer sextet lines are shown on expanded scales, compared to those of the usual bulk oxides. The problem with such comparisons with ideal bulk end-members is that the Mössbauer signal is usually sensitive to: chemical substitutions such as Fe/Ti in titanomagnetites, site occupancies and chemical order such as with the A and B sites in magnetite, particle size effects, and crystalline quality. Much of this uncertainty can be removed by going to low temperatures as others have done.

Nonetheless, it is clear from Fig. 3 that the RT magnetic mineral contribution to L4 can be almost entirely attributed to hematite. By comparison, S3 contains the same magnetic spectral component (hematite) as L4 and in about the same amount, however, S3 has extra magnetic species that have smaller hyperfine magnetic field splittings consistent with those expected for non-stoichiometric hydrous hematites (Dang *et al.* 1998), maghemites, and altered non-stoichiometric magnetites. Our whole-sample RT Mössbauer spectra clearly show that the main difference between S3 and L4, in terms of Fe-bearing mineral phases that are magnetically ordered at RT, is that S3 contains these extra magnetic species that are typical pedogenic oxides. This gives firm microscopic corroboration to several mineral magnetic studies that report extra ferrimagnetic pedogenic oxides in the paleosols.

Fig. 4 shows the magnetic susceptibility versus temperature for bulk samples of S3 and L4. An expanded scale shows the unambiguous Verwey transition of stoichiometric magnetite at 120 K in L4. Such a Verwey transition is expected to occur only in highly crystalline stoichiometric magnetite (Ozdemir *et al.* 1993) and the characteristic signature of the transition is not seen in S3. Banerjee *et al.* (1993) and Eyre and Shaw (1994) also

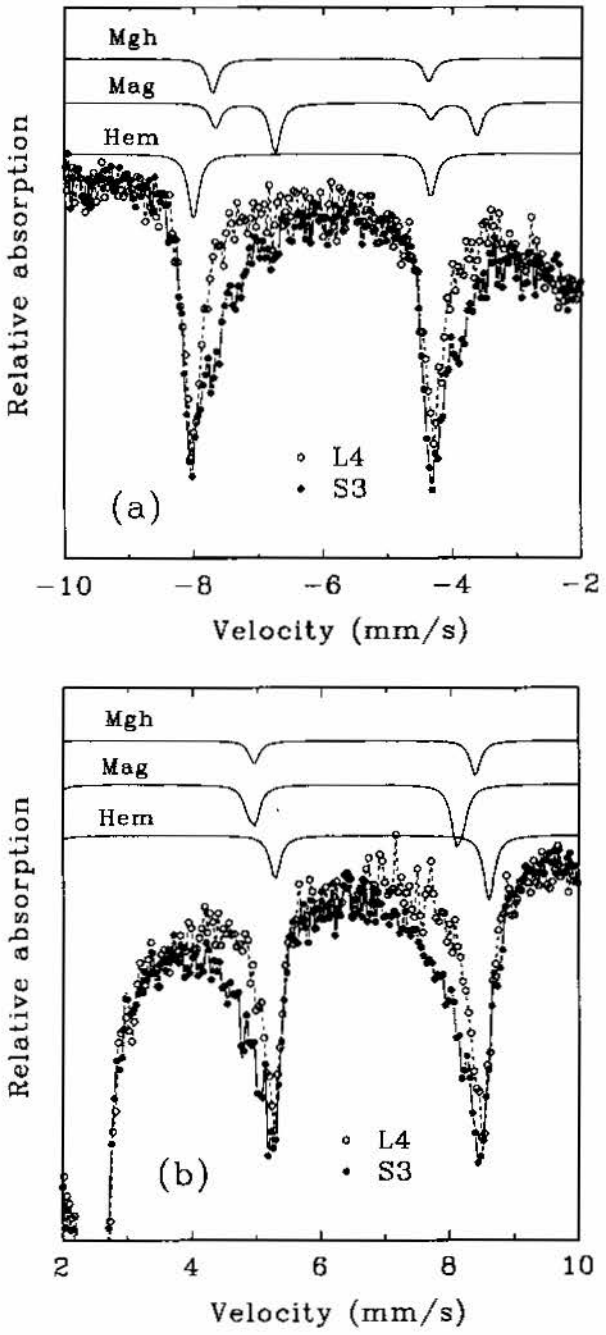

Fig. 3. Expanded views of RT Fe-57 Mössbauer spectra for whole samples S3 and L4: (a) lines 1 and 2 of hyperfine sextets; (b) lines 5 and 6 of hyperfine sextets. The two spectra are scaled such as to have equal total spectral areas for S3 and L4 (since total Fe is the same, Table 1). Simulated comparison spectra are for ideal maghemite (Mgh), magnetite (Mag), and hematite (Hem), as indicated.

observed a Verwey transition only in loess and not in paleosol. This suggests that most original lithogenic magnetite that was present in the soil (as it is in the loess) has been altered (oxidized) by pedogenic processes, however it is also possible that the lithogenic magnetite signal in

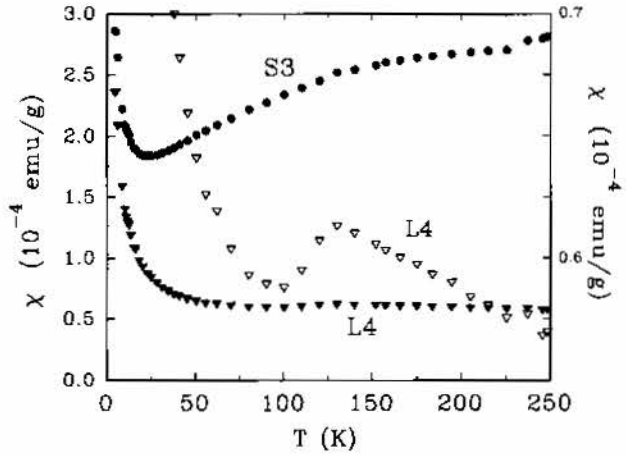

Fig. 4. SQUID magnetometry FW susceptibilities (M/H in low applied field) versus temperature for whole samples S3 and L4, on the same scale (filled symbols, left axis). The open triangles show the data for L4 on an expanded susceptibility scale (right axis).

paleosols is masked by a larger signal from pedogenic oxides. Kletetschka and Banerjee (1995) report mineral contributions with distinct Verwey transitions in both loess (100 K) and paleosol (115 K) and attribute the higher Verwey transition temperature in the paleosol to heating (and reduction) from natural fires during formation.

The FW susceptibilities (Fig. 4) clearly demonstrate that S3 has a much larger contribution from ferrimagnetic species than L4 which has an almost classic Curie behaviour corresponding to paramagnetism (Fig. 5). At low temperatures S3 also has Curie behaviour. The extracted Curie constants are 6.8 X 10^{-4} emu.K/g for S3 and 9.4 X 10^{-4} emu.K/g for L4. These Curie tails are mostly due to the paramagnetic ions (mostly Fe^{3+}, as seen in the Mössbauer spectra) that are not locked up into antiferromagnetic and ferrimagnetic species (oxides) but rather mostly reside in chlorite and illite/mica phases that have magnetic ordering temperatures below 4.2 K. The Curie tails may also have minor contributions from oxide particles that are SP at low temperatures. Such contributions are expected to suppress the Curie constants, relative to the theoretical value assuming all magnetic moments to be paramagnetic. Assuming all contributing moments are paramagnetic, the above Curie constants translate to 1.7 (L4) and 1.3 (S3) wt% Fe_2O_3 that contributes to the paramagnetism. This can be compared to the bulk amount of Fe_2O_3 of 6.1 wt% for both S3 and L4 (Table 1).

The comparison shows that, in agreement with XRD and Mössbauer spectroscopy, iron is distributed away from chlorite and illite/mica and towards the oxides in going from a loess to a soil. Indeed, a second look at the XRF results (Table 1) is also consistent with this mechanism since Na and K, which are present in micas, have relative deficiencies in S3, where they would have been freed from the micas and leached out by percolating rain water.

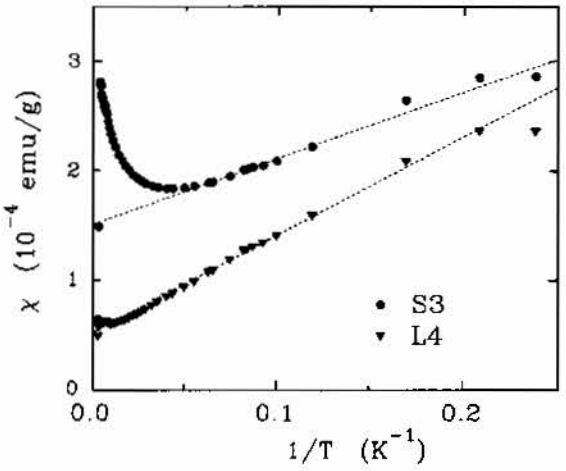

Fig. 5. SQUID magnetometry FW susceptibilities (M/H in low applied field) versus 1/T for whole samples S3 and L4. The dotted straight lines are guides to the eye that illustrate our Curie paramagnetism analyses of the low temperature Curie tails.

CONCLUSION

Our main conclusions are as follows. (1) Mineralogical phase analysis shows that the original parent material was vertically homogeneous across S3 and L4. (2) Whole-sample RT Mössbauer spectra show that the main difference between S3 and L4, in terms of Fe-bearing mineral phases that are magnetically ordered at RT, is that S3 contains extra magnetic species (non-stoichiometric hydrous hematites, maghemites, and altered non-stoichiometric magnetites) that are typical pedogenic oxides. (3) The original higher degree of pedogenic activity in the paleosol has caused a re-distribution of Fe (compared to the loess) from the chlorites and illites/micas to the pedogenic oxides, leaving the resistant minerals unaffected. (4) The most abundant Fe-oxide that is magnetically ordered at RT in L4 is hematite and a comparable amount of such hematite is also present in S3. (5) L4 also contains a relatively much smaller amount of stoichiometric (lithogenic) magnetite and a comparable amount of such lithogenic magnetite may be present in S3 although it does not give the expected Verwey magnetometry signal seen in L4. (6) S3 is anomalously Ca-rich, in comparison to L4, and this may be due to the precise location of our S3 sample, in the middle loess subunit of S3 known as LL1 (or Bt1). (7) L4 is P-rich, compared to S3, and this is tentatively explained in terms of higher pedogenic activity in the paleosol accompanied by leaching out and precipitation in the loess. (8) Finally, S3 seems to have more residual organic matter than L4, as evidenced by a higher L-O-I and a higher C content that is significantly more than can be accommodated in the calcite ($CaCO_3$).

ACKNOWLEDGMENTS

We thank the Natural Sciences and Engineering Research Council of Canada for financial support.

REFERENCES

Banerjee, S.K., Hunt, C.P. and Liu, X.-M. 1993. Separation of local signals from the regional paleomonsoon record of the Chinese loess plateau: a rock-magnetic approach. Geophysical Research Letters. **20**: 843-846.

Beer, J., Shen, C., Heller, F., Liu, T., Bonani, G., Dittrich, B., Suter, M. and Kubik, P.W. 1993. 10Be and magnetic susceptibility in Chinese loess. Geophys. Res. Lett. **20**:57-60.

Bronger, A. and Heinkele, Th. 1990. Mineralogical and Clay mineralogical aspects of loess research. Quaternary International. **7/8**: 37-51.

Dang, M.-Z., Rancourt, D.G., Dutrizac, J.E., Lamarche, G. and Provencher, R. 1998. Protohematite-hydrohematite- hematite structuro-chemical phase relationships in hematite-like materials. ICC'97, these proceedings.

Ding, Z., Yu, Z., Rutter, N.W. and Liu, T. 1994. Towards and orbital time scale for Chinese loess deposits. Quaternary Science Reviews. **13**: 39-70.

Evans, M.E. and Heller, F. 1994. Magnetic enhancement and palaeoclimate: study of a loess/palaeosol couplet across the loess plateau of China. Geophys. J. Int. **117**: 257-264.

Evans, M.E., Ding, Z. and Rutter, N.W. 1996. A high-resolution magnetic susceptibility study of a loess/palaeosol couplet at Baoji, China. Studia Geoph. et Geod. **40**: 225-233.

Eyre, J.K. and Dickson, D.P.E. 1995. Mössbauer spectroscopy analysis of iron-containing minerals in the Chinese loess. J. Geophys. Res. **100**: 17925-17930.

Eyre, J.K. and Shaw, J. 1994. Magnetic enhancement of Chinese loess – the role of gamma-Fe O. Geophys. J. Int. **117**: 265-271.

Heller, F. and Evans, M.E. 1995. Loess magnetism. Reviews of Geophysics. **33**: 211-240.

Hus, J.J. and Bater, B. 1993. Magnetic hysteresis parameters of bulk samples and particle-size fractions of the Loess/Palaeosol sequence in central China. Geologica Carpathica. **44**: 325-333.

Kletetschka, G. and Banerjee, S.K. 1995. Magnetic stratigraphy of Chinese loess as a record of natural fires. Geological Research Letters. **22**: 1341-1343.

Kukla, G. 1987. Loess stratigraphy in Central China. Quat. Sci. Rev. **6**: 191-219.

Kukla, G. and An, Z. 1989. Loess stratigraphy in Central China. Palaeogeogr., Palaeoclimatol., Palaeoecol. **72**: 203-225.

Lamarche, G. 1989. Simple top-loading cryostat insert for a SQUID magnetometer. Rev. Sci. Instrum. **60**: 943-945.

Ozdemir, O., Dunlop, D.J. and Moskowitz, B.M. 1993. The effect of oxidation on the Verwey transition in magnetite. Geophysical Research Letters. **20**: 1671-1674.

Rancourt, D.G. and Ping, J.Y. 1991. Voigt-based methods for arbitrary-shape static hyperfine parameter distributions in Mössbauer spectroscopy. Nucl. Instrum. Meth. Phys. Res. B **58**: 85-97.

Rutter, N., Ding, Z., Evans, M.E. and Liu, T. 1991. Baoji-type pedostratigraphic section, loess plateau, north-central China. Quaternary Science Reviews. **10**: 1-22.

Vandenberghe, R.E., de Grave, E., Hus, J.J. and Han, J. 1992. Characterization of chinese loess and associated paloeosol by Mössbauer spectroscopy. Hyp. Int. **70**: 977-980.

Vandenberghe, R.E., de Grave, E., Hus, J.J. and Han, J. 1998. Study of Chinese loess and associated paleosols by Mössbauer spectroscopy. ICC'97 procedings and HI special issue.